Extrinsic effects on the disorder dynamics of Bénard-Marangoni patterns

P. Cerisier,[1] S. Rahal,[1] and B. Billia[2]
[1]*IUSTI, UMR CNRS 139, University of Provence, 13397 Marseille Cedex 20, France*
[2]*Laboratoire MATOP, CNRS, Faculté des Sciences et Techniques de Saint Jérôme, University of Aix-Marseille III, Case 151, 13397 Marseille Cedex 20, France*
(Received 9 April 1996)

The influence of the vessel shape, the initial conditions, and the vertical temperature gradient on dynamics and amount of disorder in convective patterns evolving in Bénard-Marangoni instability have been analyzed by using statistical tools, namely the density of defects, a disorder function, the order-disorder (m,σ) diagram introduced from the minimal spanning tree approach by Dussert *et al.*, [Phys. Rev. B **34**, 3528 (1986)] and the entropy function recently defined by Loeffler (unpublished). Pattern disorder is studied for transient and steady states. Experimental results show that the disorder in the hexagonal patterns of Bénard-Marangoni convection (i) is minimized in a hexagonal vessel and (ii) can be described as a Gaussian noise superimposed on a perfect array of hexagonal cells. Starting from imposed arrays, both hexagonal and nonhexagonal, with a wavelength different from the one that is naturally selected, the final state is independent of initial conditions. Disorder increases with the distance from the threshold. Depending on the Prandtl number, different behaviors of the patterns are observed. [S1063-651X(96)08210-4]

PACS number(s): 02.50.−r, 05.45.+b, 47.54.+r, 64.60.Cn

I. INTRODUCTION

The spatiotemporal behavior of spatially extended, dissipative systems with significant fluctuations in both space and time has been intensively studied in recent years [1]. An important problem in the study of these complex systems is that of finding suitable methods for their analysis. Statistical rather than deterministic methods have often been used for experimental studies [2–5].

A prototype of these complex systems is given by the Rayleigh-Bénard problem. In this instability, a pattern of rolls develops, as seen in experiments and in weakly nonlinear analyses. Irregularities are generally present in these patterns, including dislocationlike defects and orientational disorder [6]. These complicated patterns may be characterized by a two-dimensional horizontal wave-vector field that, from the theoretical point of view, can be obtained from an amplitude equation [7].

In the Bénard-Marangoni (BM) case, a pattern of hexagons is the most stable structure in usual situations [8]. Such patterns often exhibit some topological defects that are mainly pentagon-heptagon pairs and aggregates of irregular polygons [9]. It is noteworthy that these defects are also observed in different natural hexagonal structures; for example, in honeycombs, crystals, liquid crystals, or interfacial patterns during solidification [10]. It is widely recognized that simple, regular, and symmetric patterns are exceptional in convection experiments [11].

To our knowledge, in the scarce theoretical analysis completed up to now in BM convection, the dynamics of these irregular patterns have not been analyzed. Until now, only experimental studies exist [11–13] in which the formation and evolution of defects (mutual transformation, annihilation) in hexagonal patterns are described. As a complete theory of defect dynamics is still lacking, it has proven useful to use the analogy between these patterns and monolayered materials in two dimensions [14]. Within this framework, Occelli *et al.* [15] have proposed a quantitative description of spatial disorder using a radial correlation function and an orientation correlation function, theoretical tools that are used to describe melting in two-dimensional 2D hexagonal lattices, i.e., structures at the atomic level. Although similarities between 2D structures and BM patterns exist, it must be noted that the differences are very stringent. The main ones are that 2D layered structures are static, whereas convective patterns are a purely dynamical creation and formed by convective cells whose number is not conserved; i.e., cells can be created or annihilated (the total number of cells in the pattern suffers small fluctuations even in ''steady'' states).

The question of disorder in cellular patterns, which plays an essential role in the apparition of turbulence and in the transition to chaos [16], is linked to the fundamental problem of wavelength selection [17,18]. Is selection weak or sharp? Do preferred patterns exist or not? These are central issues in pattern-forming instabilities [1]. There are several ways to quantify disorder in patterns, which all depend on the definition of disorder itself. The easy and obvious way is to identify, classify, and count the defects, which are simply defined as the cells whose number of sides differs from six. It follows that the density of defects, i.e., the ratio of the number of defects to the total number of cells, is one major measure of disorder. Nevertheless, it is a global parameter that does not take into account the pattern distortion. Indeed, in particular, in small vessels, an irregular pattern can be observed only due to the presence of irregular hexagons; in that case the density of defects is zero and yet the pattern is not regular. To take into account the whole pattern distortion, a disorder function F_d has been introduced [11].

We have proposed [19] to use an alternative and more informative method to study the disorder in a BM pattern, namely the minimal spanning tree MST approach. This approach was introduced by Dussert *et al.* [20] to study the organization in a thin film of aggregated lithium deposited on

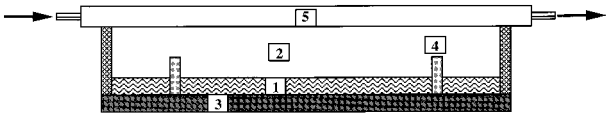

FIG. 1. Schema of the experimental setup. 1, fluid layer; 2, air; 3, container; 4, vessel; 5, cooling container.

a dielectric substance. It was then used by Billia *et al.* [21] to carry out the statistical analysis of the topological defects and disorder that occur in directional solidification of cellular and dendritic arrays resulting from the morphological instability of the planar solid-liquid interface.

The aim of this work is to use statistical tools to analyze the effects of external parameters (vessel shape, initial conditions, vertical temperature gradient, Prandtl number (Pr), etc.) on the amount and on the dynamics of disorder in BM patterns. The experimental procedure is described in Sec. II. Section III is devoted to the description of the statistical tools; results are given and discussed in Sec. IV; and, finally, major conclusions are gathered in Sec. V.

II. EXPERIMENTAL PROCEDURE

The experimental setup consists of a thin (4.3-mm) horizontal layer of silicon oil, Rhodorsil 47V50 or 47V100 (corresponding respectively to $Pr_1=440$ and $Pr_2=880$ at 25 °C), contained in a vessel with a flat copper bottom (in which an electric resistance is embedded to provide a uniform temperature) and lateral walls made of Plexiglass, which has about the same thermal conductivity as the silicon oil. The vessel, which limits laterally the part of the layer under study, is surrounded by an outer guard ring of the same oil. The presence of this ring guarantees a quasiadiabaticity of the sidewalls. The fluid was cooled from above through an air layer. The air was bounded on top by a glass plate, which is the bottom of a container in which water, coming from a bath with regulated temperature, circulates in order to fix the temperature of the glass plate and thereby the temperature on top of the fluid. The essential features of the apparatus described above are shown in Fig. 1. The temperatures at the upper and lower surfaces are measured by means of thermocouples; the precision of the measurements is about 0.1 °C. The liquid depth (d) is measured by means of micrometer comparators with a precision of 0.01 mm. Flow visualization is achieved by aluminum flakes suspended in the fluid. Photographs of the convective structure are taken at regular time intervals during a long period. Then each photograph is digitized. Appropriate filterings and scalings provide a binary image, which is skeletonized later (Fig. 2). Then, a suitable software is written that allows us to obtain the values of the relevant functions used in the statistical analysis.

The confinement is taken into account by means of a nondimensional parameter, the aspect ratio $\Gamma=\sqrt{A}/d$, which is the ratio of a characteristic horizontal length of the fluid layer $\sqrt{A}$, with A the surface area of the pattern, to the liquid depth (d). Experiments have been performed in vessels with Γ between 65 and 85, the first value corresponds to medium final confinement [22]; Under these conditions, wall effects exist but do not induce large extrinsic disorder, and mobility of the structure is allowed as well as the existence of intrinsic disorder.

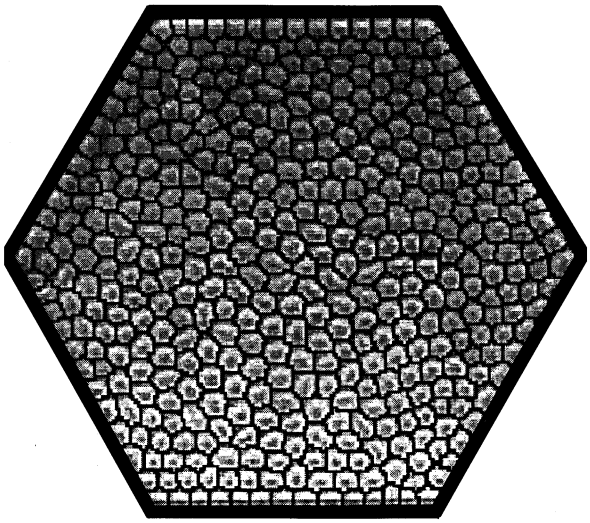

FIG. 2. Superposition of the skeletonized cellular array on the picture of a cellular array in Bénard-Marangoni convection.

The external parameter that controls the instability is the vertical temperature difference ΔT across the layer. Usually, it is more useful to take a normalized parameter, the distance to the threshold:

$$\varepsilon=\frac{R-R_c}{R_c}=\frac{M-M_c}{M_c}, \tag{1}$$

where R and M are, respectively, the Rayleigh and Marangoni numbers, and the subscript c stands for the corresponding threshold value.

Three series of experiments were carried out.

(i) Experiments are performed in hexagonal (V_h), circular (V_c), or in square (V_s) vessels, for the same physical parameters (distance to the threshold $\varepsilon=0.05$, aspect ratio $\Gamma=85$, Prandtl number Pr_2). First, the liquid is stirred up. Then, the pattern self-organizes progressively until the final steady state is reached. The characteristics of the structures obtained in the various vessels will be compared in Sec. IV A. The experimental results of series (i) convinced us to perform two other series of experiments in a hexagonal vessel with $\Gamma=65$ corresponding to medium confinement.

(ii) Thanks to the thermal marking technique described in detail in [23], regular arrays of cells can now be imposed as initial conditions. In practice, hexagonal arrays with a cell size equal to or larger than the ''natural'' one (i.e., the mean size selected in the steady regime) as well as triangular or square patterns are also initially forced. The self-organization of the pattern from the initial almost perfect state up to the final one (regular or disordered hexagonal structure) is studied. Experiments are performed in a hexagonal vessel with $\Gamma=65$ and for $Pr_2=880$ at 25 °C.

(iii) Various experiments corresponding to various values of ε and to Pr_1 and Pr_2 are performed. Initially, there is no imposed structure, but a complete mixing of the fluid by stirring it up. Transient and steady regimes are studied.

III. TOOLS USED FOR THE ANALYSIS OF THE DISORDER

A. Density of defects

The density of defects d_d is defined as the ratio of number of defects n_d (cells whose number of sides differs from six) to the total number of cells (N). As already underlined, defects are chiefly pentagons (P_5) and heptagons (P_7) in steady states, so that the density of defects is, in that condition, well approximated by

$$d_d = \frac{n(P_5)+n(P_7)}{N}. \tag{2}$$

B. Disorder function

The density of defects [11] and the orientation and translation correlation functions [15] are only useful when patterns have a number of cells that are sufficient to make statistics reliable. In small vessels, with only a few cells, the structure can display no defect and almost regular hexagons (Fig. 1 in Ref. [11]), whereas some distortion is still present in the pattern. Therefore, in this situation, a quantitative measure of distortion is necessary to estimate the amount of pattern disorder. For this, the following function has been proposed [11]:

$$F_d = \frac{1}{2N}\sum_{i=1}^{N}\frac{1}{n_i}\sum_{j=1}^{n_i}\left|\ln\frac{l_i}{l}\right|, \tag{3}$$

where N is the number of cells in the pattern, n_i is the coordination number of the ith cell, l_{ij} is the distance between the center of the ith cell, and the center of its jth neighbor, and l stands for the length between the centers of nearest-neighbor cells averaged over the whole pattern (for this average, only hexagonal cells are taken into account). F_d is an average of the deviations of the distance between the cell centers with respect to a completely regular pattern. In analogy with the entropy in regular honeycomb lattices [24], a logarithmic function has been chosen. The absolute value is taken in order to have contributions that do not cancel each other when the length between two centers is smaller or larger than the mean value. These contributions are averaged over the nearest neighbors and, finally, all these contributions are added over the whole pattern. Note that with this function one can also account for distortions in patterns with very few convective cells.

C. Minimal spanning tree (MST) approach and entropy function

Some years ago, Dussert *et al.* [20] proposed a new method based on principles of graph theory, the minimal spanning tree (MST) approach, to analyze order and disorder in a distribution of points. Data in the form of a set of points, spread within a region of space, arise in many fields such as astronomy, crystallography, solid-state physics, biology, etc. It is often possible to consider the objects to be studied (stars, elementary particles, aggregates, proteins, etc.) as points and thus to treat such a data set as a distribution of points on a surface.

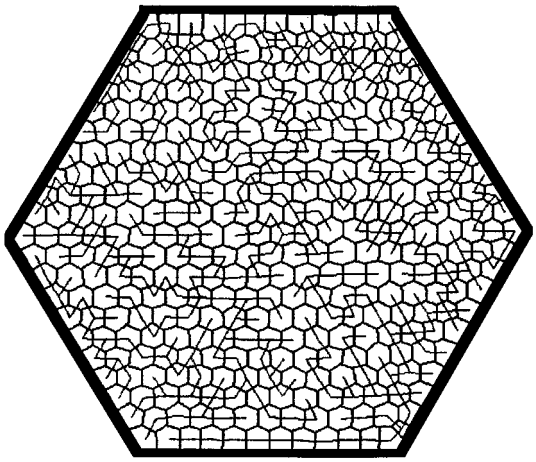

FIG. 3. The minimal spanning tree (MST) superimposed on the 2D Bénard-Maragoni array in a hexagonal vessel.

Graph theory is well developed and applied in a large variety of fields, so that the basic definitions can be easily found elsewhere [25–27]. Therefore, the following presentation is reduced to a minimum. Let us recall that an edge-weighted linear graph is composed of a set of nodes (the cell centers for the case of cellular arrays) and a set of edges, an edge being defined by a pair of cell centers, with a weight assigned to each edge (the corresponding center-to-center distance). A MST is a connected graph without any closed loop, which contains all the cell centers and for which the sum of the edge weights is minimum. One starts from any cell center and adds at each step the cell center that is closest to the current tree (Fig. 3). A MST can be constructed for any distribution of points on a surface. It should be emphasized that the MST does not contain all the first-neighbor distances but a selected subset of $N-1$ elements.

There are a few specific cases in which there exist some edge lengths that are equal, so that, for a given distribution of cell centers, the MST may not be unique and locally vary, depending on the point that is selected to start its construction. Nevertheless, the important property is that all the possible MST's are equivalent in the sense that the edge-length histogram is unique. This fact legitimates the utilization of parameters that are deduced from the statistical analysis of that histogram to characterize the arrangement of the cell centers. The most informative parameters are linked to the moments of the distribution, the two major ones being the average edge length m^* and the standard deviation σ^*. It was shown by Dussert *et al.* [20,27] that it is most convenient to normalize m^* and σ^* as

$$m = \frac{m^*}{\sqrt{\langle a\rangle}}\frac{N-1}{N}, \tag{4}$$

$$\sigma = \frac{\sigma^*}{\sqrt{\langle a\rangle}}\frac{N-1}{N}, \tag{5}$$

where N is the total number of cells and $\langle a\rangle$ the averaged cell area.

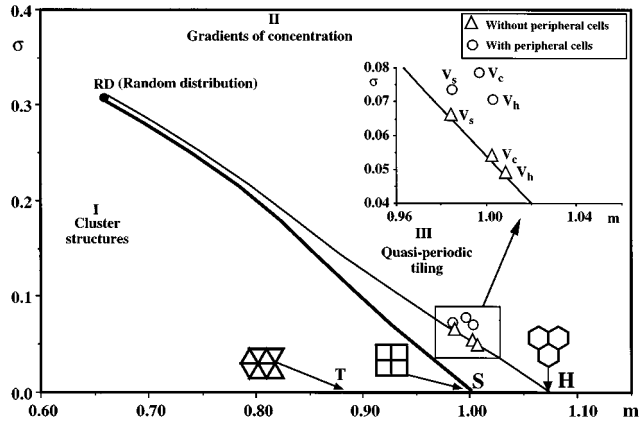

FIG. 4. The (m,σ) diagram. m, normalized averaged length; σ, normalized standard deviation of the edge-length histogram. The three major areas (I, II, and III) and three typical perfect mosaics (T, triangular; S, square; and H, hexagonal) are shown. RD corresponds to the computed random distribution. Computed curves joining RD to S and to H are also visible. Inset shows the representative points of whole patterns and patterns without peripheral cells for various arrays in various vessels. V_h, hexagonal vessel; V_c, circular vessel; V_s, square vessel. $\Gamma=85$, $\varepsilon=0.05$.

By doing this, any distribution can be plotted in the (m,σ) plane (Fig. 4), where it can be compared to any other two-dimensional (2D) arrangement. Three lattices (triangular T, square S, and hexagonal H) among the 11 possible regular mosaics ($\sigma=0$) and the random distribution (RD) are shown in the (m,σ) plane. Dussert *et al.* [20,27] have progressively randomized regular lattices by giving each point a new position deduced from its previous one using a Gaussian distribution of displacements of increasing standard deviation. The computed trajectories joining S and H to RD are also shown in Fig. 4. The areas marked I, II, and III on the diagram of Fig. 4 respectively correspond to cluster structures (small m, $\sigma\neq0$) [26], gradients of concentration (large σ), and 2D quasiperiodic tilings (large m, $\sigma\neq0$) [28]. It follows that by construction of the MST, normalizing and plotting in the (m,σ) plane, one is able to determine the underlying arrangement of the 2D cellular arrays, i.e., to elucidate order behind disorder, and measure disorder, particularly when representative points fall on computed lines.

The edge-length histogram contains somewhat more statistical information than the (m,σ) couple, so that it is tempting to directly use it. One might think it useful to also take into account the complementary information that can be extracted from the MST by considering the histogram of angles, the angles being those made by the MST edges with respect to an arbitrary direction [27]. Yet the histogram of angles is not unique when there are several possible MST's, so that it has to be discarded when seeking some thermodynamic function enabling a sound hierarchy in the patterns. Based on the edge-length histogram, an entropy function $S(1)$ has been recently introduced [29]:

$$S(1)=-\sum_i p(l_i)\ln[p(l_i)], \tag{6}$$

where $p(l_i)$ is the proportion of edges with a length in the class $(l_i\pm\Delta1)$.

IV. RESULTS AND DISCUSSION

A. Influence of vessel shape on the patterns

The influence of vessel shape on the structure of BM convection was pointed out by Bénard himself as early as 1901. The sidewalls act on the structure, especially for small vessels, by the existence of a meniscus that locally modifies the depth layer and by boundary conditions on the velocity and on the temperature (or the heat flux). The most striking consequence of the wall presence is that the cell edges in contact with the walls are perpendicular to them in the steady regime. It is obvious that the smaller the vessel the larger the influence of sidewalls on the whole structure.

From a general point of view, in Rayleigh-Bénard convection, the wave-number selection depends on boundary conditions [30]. One should be reminded of papers by Pomeau and co-workers [17,31,32] and by Davis [33,34] in which it is specified that when the aspect ratio increases, the number of permitted modes also increases due to the weakening of the strength of the finite-size effect. Also, in BM patterns, the condition of orthogonality to the sidewalls of convective-cell sides in contact can be satisfied only in hexagonal and equilateral triangular vessels. Indeed, in a compatible vessel, this condition of orthogonality can be satisfied from a geometrical point of view. The pattern is composed of regular hexagons in the central part and of rows of pentagons on the periphery. Experiments show that these outer cells are stable; they do not induce any disorder in the pattern. All other containers, such as square, rectangular, pentagonal, circular, ring or crescent-shaped vessels, are geometrically incompatible with a perfect convective pattern [11–13]. In these vessels, some distortion of the pattern with the concomitant presence of topological defects is necessary to conciliate the various directions imposed by the walls. For instance, relying on the space-filling argument, Rivier *et al.*

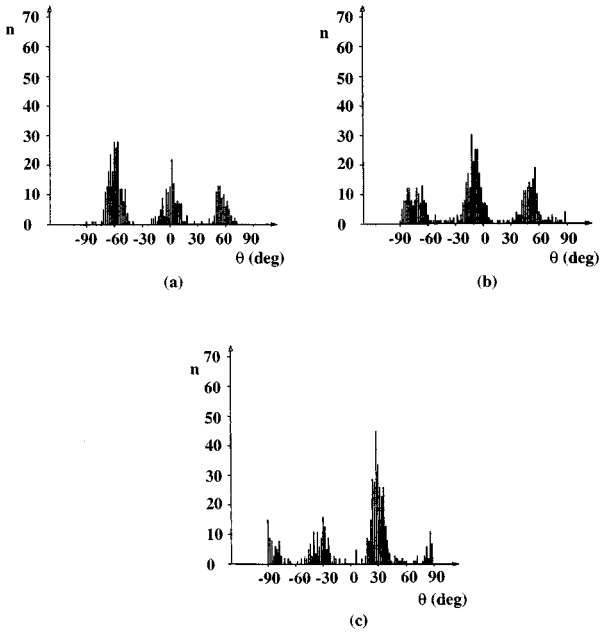

FIG. 5. Histograms of angles of the minimal spanning tree: (a) hexagonal (b) circular, and (c) square vessels (without peripheral cells).

TABLE I. Values of d_d, F_d and $S(1)$ for various vessels. $\Gamma=85$, $\varepsilon=0.05$.

	All cells considered			Peripheral cells excluded		
Vessel	d_d (%)	F_d	$S(1)$	d_d (%)	F_d	$S(1)$
Hexagon	0.15	0.052	3.23	0.033	0.052	2.97
Cylinder	0.16	0.051	3.33	0.086	0.051	3.25
Square	0.18	0.066	3.26	0.092	0.067	2.98

[35] showed theoretically that a hexagonal arrangement in a circular vessel must contain at least six positive disclinations [36] or pentagonal cells in the midst of the array.

In Fig. 5, the histograms of angles of the MST corresponding to the various vessels are displayed. The reference direction is horizontal, i.e., parallel to two vessel walls in V_h or in V_s. It can be seen that the characteristic directions of the hexagonal pattern oriented to each other by 60° are clearly exhibited. The angles are obviously 0°, +60°, and −60° in V_h, in conformity with the orthogonality condition for marginal cells. On the other hand, the orientation of the pattern in V_c is random. This is a direct consequence of the extension of the Curie principle to dynamical systems [37]: one realization breaks circular symmetry but the average over many experiments, or time averaging, should restore it, which was verified in other symmetry-breaking instabilities [38,39]. In V_s, angles at ±90° are visible. This is due to the fact that in V_s short distances between cell centers, which are retained in the construction of the MST, are rather perpendicular to the reference direction for the case shown, although the two directions imposed by the square walls have the same probability. Indeed, we performed other experiments and we remarked that short edges can be parallel or perpendicular to the reference direction.

Experimental results for d_d, F_d, and $S(1)$ in steady states for series (i) are listed in Table I; the total number of cells is about 570 when cells in contact with the vessel walls are taken into account and about 490 when they are excluded (vessels have the same aspect ratio but the total numbers of cells are not strictly equal). It can be seen that the variation of the density of defects d_d, minimum for the hexagonal vessel (V_h), and maximum for the square vessel (V_s) is in conformity with the topological considerations in the preceding paragraph. In natural convective patterns, some defects that have a dynamic origin, are always present in large hexagonal vessels, although they are, in principle, compatible. Even if the density d_d is greater in V_c than in V_h, the strains induced by cylindrical symmetry seem to be uniformly distributed over the pattern as the distortion in the lattice, measured by F_d, is small. Indeed, taking these two effects together (more defects but fewer strains from walls; there are no angles) could explain why F_d is about the same for V_c and for V_h. For V_s, F_d is significantly higher, in agreement with higher incompatible symmetry. The entropy function $S(1)$ inverts the above classification between V_c and V_s. Indeed, Table I again shows that V_h is the most adapted vessel but the shortest edge lengths are found to be more disordered in V_c than in V_s, the effect being clearer when outer cells are excluded.

Figure 4 shows that in the (m,σ) plane disorder increases according to the sequence V_h, V_c, V_s. When peripheral cells are not taken into account, the three representative points fall on the line H-RD, so that the total (topological+stretching) disorder can be described as a Gaussian noise perturbing an ideal hexagonal planform. When peripheral cells are taken into account, representative points are above the line H-RD, which means that these cells, truncated by wall constraints, belong to another category. Actually, the outer cells introduce shorter edge lengths that are preferred in the construction of the MST. The detrimental consequence is that the statistical analysis is then biased when the aim is to discover characteristics representative of planforms in an extended system.

B. Influence of initial conditions on pattern dynamics and order-disorder transition

Experiments of series (ii) and (iii) have been performed in a hexagonal vessel because series (i) showed that this shape induced a minimum extrinsic disorder. The aspect ratio $\Gamma=65$ has been chosen to induce moderate wall effects on the pattern [22]. Indeed, if the aspect ratio is small, the pattern has no structural defects, even for moderate ε. On the contrary, if it is large, the layer can be considered as infinitely extended in the horizontal directions and the vessel has no larger influence. The value $\Gamma=65$ provides stabilized wall effects limited to a few cell rows (1 to 3) near the walls and allows the structure to evolve freely in its central part.

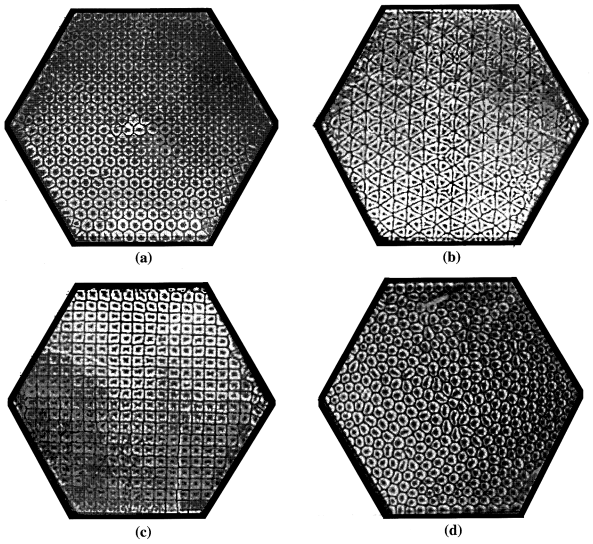

FIG. 6. Initial and final patterns of series 2. $\Gamma=65$, $\varepsilon=4.5$. (a) Initial pattern of case 2.1; (b) initial pattern of case 2.3; (c) initial pattern of case 2.4; and (d) final pattern of case 2.4, statistically equivalent to final patterns of cases 2.2 and 2.3.

It is interesting to investigate the influence of initial conditions on the characteristics of the final cellular arrays in order to go deeper into an understanding of the mechanisms of wavelength selection that may arise from the dynamics of the pattern itself. This point is emphasized by Cross and Hohenberg in their review of pattern formation outside of equilibrium [1]. In particular, they discuss the meaning of selection, which leads them to introduce the notion of ''preferred'' state for systems for which there is no evidence of an ordering principle. Namely, one state is ''preferred'' if it has a larger basin of attraction for *typical* initial conditions, or if it evolves from an initial condition where different states coexist side by side. These authors conclude that such considerations naturally direct the attention to the specific way in which the control parameters reach their final values and to the dynamics leading to the final steady state. In that goal we performed series-(ii) experiments with various imposed initial structures ($\Gamma=65$ and $\varepsilon=4.5$).

Case 2.1: regular hexagonal pattern with wavelength $\lambda_i \approx \lambda_f$ (i, initial; f, final),

Case 2.2: regular hexagonal pattern with wavelength $\lambda_i > \lambda_f$,

Case 2.3: triangular pattern,

Case 2.4: square pattern.

For experiments 2.3 and 2.4, imposed cells have areas very close to that of hexagonal cells imposed in case 2.1.

Figure 6 shows structures very close to the prepared patterns imposed as initial conditions and a final one. It can be noticed that hexagonal array [Fig. 6(a)] is regular because the honeycomb is the natural structure and the imposed wavelength is very close to the naturally selected mean value. The triangular [Fig. 6(b)] and the square [Fig. 6(c)] patterns already show some defects (with a different meaning than before, i.e., cells with a number of sides different respectively from 3 and 4) because the imposed structures are not at all natural and the employed thermal technique displays some small imperfections due to misalignment of some cold needles [23]. We remark that many peripheral cells rapidly become perpendicular to walls for triangular and square imposed patterns. The final array corresponding to the steady

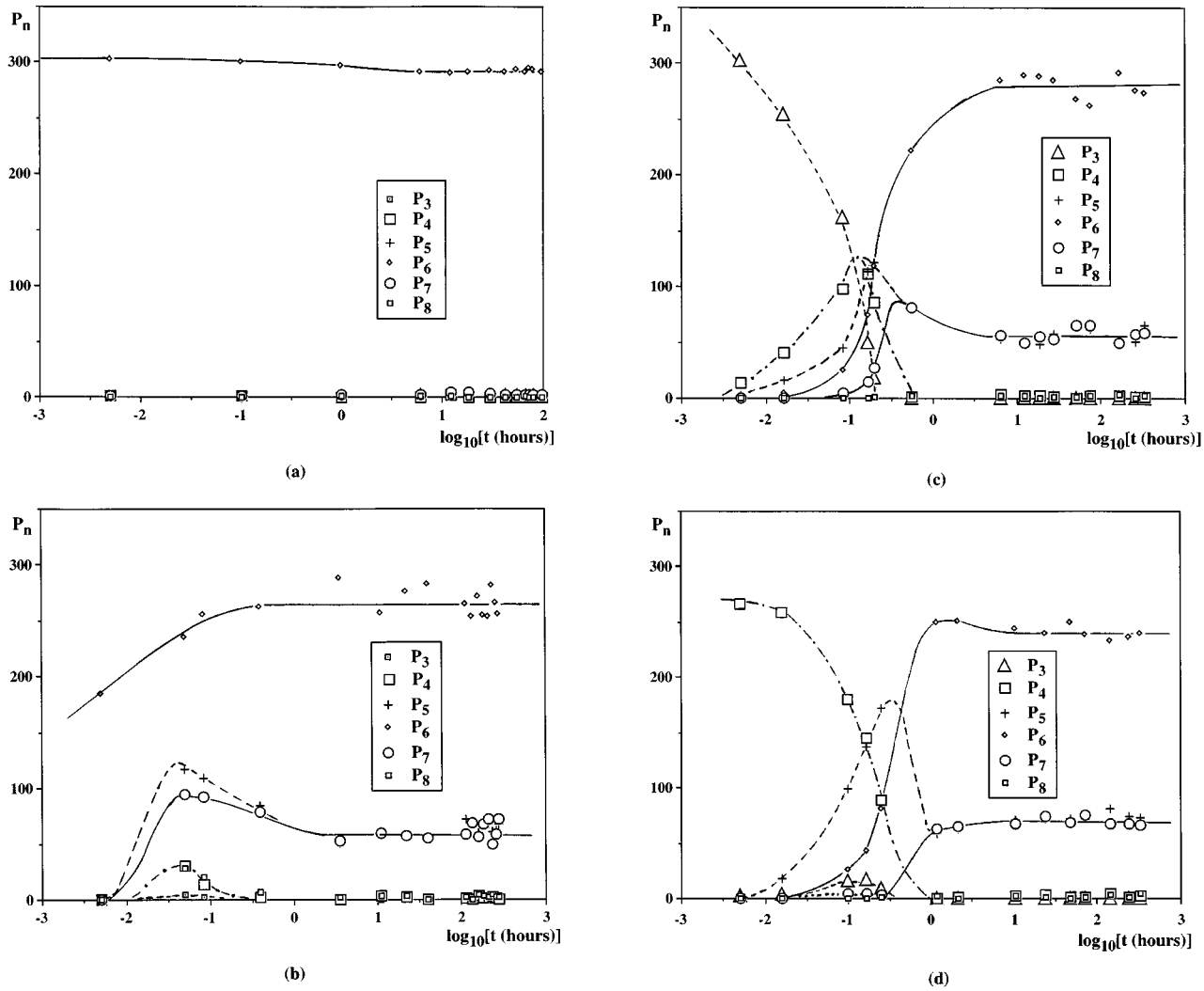

FIG. 7. Evolution of the number of polygons P_n as a function of time [series (ii)]. $\Gamma=65$, $\varepsilon=4.5$: (a) initial regular hexagonal pattern with wavelength $\lambda_i \approx \lambda_f$ (i, initial; f final), (case 2.1); (b) initial regular hexagonal pattern with wavelength $\lambda_i > \lambda_f$ (case 2.2); (c) initial triangular pattern (case 2.3); and (d) initial square pattern (case 2.4). When several symbols are superimposed some of them are hidden; the lines serve as guides to the eye.

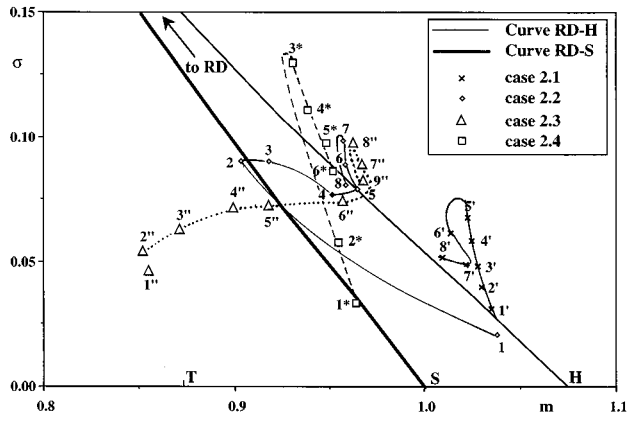

FIG. 8. Evolution of cellular arrays with time in the (m,σ) diagram for series (ii). $\Gamma=65$, $\varepsilon=4.5$. When several symbols are superimposed some of them are hidden; the lines serve as guides to the eye.

regime of experiment 2.1, which resembles Fig. 6(a), is almost a regular hexagonal array, whereas the final arrays of experiments 2.2 and 2.3 are disordered structures statistically equivalent to that of experiment 2.4 [Fig. 6(d)], as will be shown in the following.

Carried out by initially imposing a honeycomb with a wavelength *adapted* (very close to the natural one) to the level of instability, experiment 2.1 is critical. Apart from the cells close to the container walls [Fig. 6(a)], it showed no array dynamics during a long period (about 15 days). It followed that the cellular array remained quasiregular with very few topological defects and disorder that could not even be sustained when appearing in the core of the pattern. Such an experiment indicates that, in BM convection, ''limited dynamics=limited disorder,'' which leads one to conjecture that ''no dynamics=no disorder'' would be found if stretching effects were suppressed by using a hexagonal container commensurable with the imposed honeycomb spacing. We plan to ascertain this point in a forthcoming study.

Cells on the periphery being excluded, the evolution of the number of polygons P_n $(n=3,\ldots,8)$ for experiment 2.1 is shown in Fig. 7(a). The number P_6 of six-sided cells is almost constant, or in other words, the number of topological defects remains nearly zero, so that it can be considered that the dynamics of pattern formation has been reduced enough to make ''no disorder'' achievable in the d_d case. Figure 7(b), devoted to the evolution of an initially hexagonal pattern with $\lambda_i>\lambda_f$ (case 2.2), confirms the general trend: a disordered pattern contains only P_5 and P_7 as defects in the steady regime. During the partial destruction of the regular pattern, transitory P_4 and P_8 cells can appear. This is due to the large size of the imposed cells; there are divisions of P_6 cells and resulting unstable cells coalesce. When a triangular pattern is imposed as in case 2.3 [Fig. 7(c)], triangular cells disappear rapidly. After about 12 min there does not remain any P_3 cell visible to the naked eye. At the same time the P_4 are created, the P_5, P_6, and P_7 are also created. The rearrangement of the intermediate pattern, made of P_4, P_5, P_6, and P_7, leads to the usual pattern with P_6, P_5, and P_7. Figure 7(d) exhibits the same behavior when square cells are imposed. For the last three cases, the imposed patterns have totally disappeared 15 min after starting the experiment, i.e.,

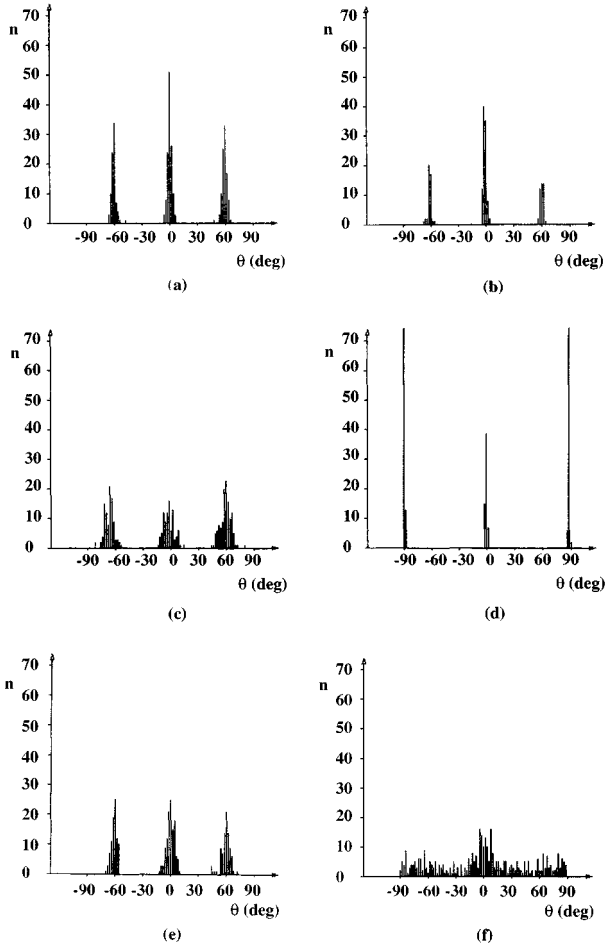

FIG. 9. The minimal spanning tree (MST): histograms of edge angles. $\Gamma=65$, $\varepsilon=4.5$. Initial patterns: (a) case 2.1, (b) case 2.2, (c) case 2.3, and (d) case 2.4. Final patterns: (e) case 2.1 and (f) case 2.4 statistically equivalent to cases 2.2 and 2.3.

2×10^4 times the viscous diffusion time $\tau_{\rm visc}$ $(=0.043$ sec for $\mathrm{Pr}_2=880$ at 25 °C) and 24 times the thermal diffusion time $\tau_{\rm th}$ $(=37.9$ sec for $\mathrm{Pr}_2)$.

In Fig. 8, we give the evolution with time of the representative points in the (m,σ) plane for the various cases of series (ii). The representative points of initial arrays of cases 2.1 (point 1), 2.2 (point $1'$) are, as expected, very close to H as they correspond to almost perfect hexagonal patterns. For case 2.3, the array (point $1''$) is initially nearby T, which locates the regular triangular structure. Similarly, for case 2.4 (point 1^*) the pattern starts close to the square mosaic S, on the computed line S-RD. It is worth noticing that, in all cases, there is a transient incursion into the adjacent region above the line H-RD. Although it is made up of six-sided cells ($d_d\approx0$), the final stage for experiment 2.1 (point 8) is not a perfect honeycomb ($m=1.01$ and $\sigma=0.051$ instead of $m=1.075$ and $\sigma=0$) but rather a distorted hexagonal pattern. For an imposed hexagonal array larger than the natural one, case 2.2, the transient regime presents a tendency to the region of square cells (points $2'$ and $3'$) that may reflect the fact that, initially, the imposed size (point $1'$) is too large and a division phase occurs. During this phase, there is a significant number of P_4 defects [see Fig. 7(b)], which is accompanied by a decrease of m and an increase of σ. A first

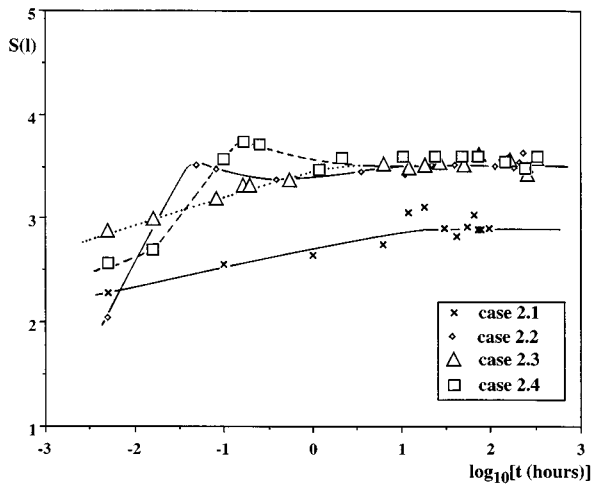

FIG. 10. Entropy $S(l)$ versus time for arrays of series (ii). $\Gamma=65$, $\varepsilon=4.5$. Peripheral cells are excluded from calculations.

period of array rearrangement follows during which dispersion, characterized by σ, decreases (point $4'$). As usual with the MST construction, the increase of m follows from the lowering of the number of very small cells, which naturally provide short edges. Moreover, during the first division stage, the system probably creates more cells than necessary so that small cell elimination occurs during the next period. Then, the process of cell division is repeated, giving rise to an oscillatory drift, in the sense of disorder, towards a quasiasymptotic pattern (point $8'$). After about 275 h, the pattern has self-reorganized into a hexagonal array more disordered than in the experiment 2.1 with initial adapted spacing, as the final point $8'$ ($m=0.96$ and $\sigma=0.081$) has moved towards RD with respect to point 8. Experiments 2.3 and 2.4 evolve rapidly towards statistically equivalent final states (points $9''$ and 6*), comparable to that in experiment 2.2.

When, in Fig. 8, representative points fall on the same computed trajectory to RD, e.g., H-RD, the absence of metrics in the (m,σ) diagram can be overcome. Then, the global distortion of the patterns can be measured by the amount of Gaussian disorder introduced in the randomization process (see Fig. 4 in Ref. [20]). The standard deviation of the distribution of the shifts from the ideal positions equals 0.045 for the asymptotic state of experiment 2.1 and 0.078 for the final state of experiment 2.2, which respectively correspond to 9.6% and 16.6% of the value for a completely random structure. Yet topological disorder is striking in Fig. 6(d) ($d_d=31\%$), whereas it is not discernible in experiment 2.1. It thus follows that the large effects, seen in the figures and measured by d_d, are produced by a small cause, which means that disorder is a highly nonlinear function of the cellular shifts that might explain why, by the MST method, it remains possible to bring forward the underlying honeycomb even at large distances from the onset of instability.

The histograms of angles for the initial states of series-(ii) experiments are shown in Figs. 9(a)–9(d). For all cases, the imposed angles are very close to the theoretical values. The final pattern keeps good orientational order for case 2.1 [Fig. 9(e)], whereas the other three initial arrays end in a similar pattern with a weakly nonuniform distribution of angles; only small and large peaks can be distinguished [Fig. 9(f)].

The entropy function $S(1)$, Fig. 10, shows that the final state is reached after about 0.2 h ($=1.8\times10^4\tau_{\rm visc}$ and $19\tau_{\rm th}$) for cases 2.2, 2.3, and 2.4, whereas it needs several hours for the evolution of polygons P_n (Fig. 7). This difference can be explained by noting that $S(1)$ nears its asymptotic value at the time the three structures 2.2, 2.3, and 2.4 adopt a similar aspect, with a majority of hexagons and essentially pentagons and heptagons as defects. Indeed, the appearance or disappearance of a few pentagon-heptagon pairs modifies strongly the density of defects but does not significantly affect the entropy because these pairs have nearly the same size and the same orientation as the two hexagons in a disordered lattice. Although the pattern in experiment 2.1 only undergoes minor modifications, the final state is eventually realized after 12 h, i.e., after about $10^6\tau_{\rm visc}$ and $10^3\tau_{\rm th}$. On general grounds, there exist several contributions to entropy, which possess different characteristic times. For case 2.1, because all the outer cells make perpendicular contacts, the wall contribution is zero, as is the case for the topological defects ($d_d\approx0$). Therefore, only the stretching, which is different from zero as the initial hexagonal pattern is adapted for wavelength but is not commensurable with the size of the hexagonal container, determines the characteristic time of the evolution of the array. Finally, it should be noticed that the common entropy value of the final states of experiments 2.2, 2.3, and 2.4 is significantly higher than that of case 2.1.

C. Influence of ε and Pr on patterns in steady regimes

We noted in Sec. IV B that a ''statistical'' final state is reached after about 12 h (at maximum). But from a general point of view we must stress that the pattern is not stationary and its characteristics fluctuate around mean values. These fluctuations are a consequence of the cell dynamics; cells can grow, evolve, and sometimes annihilate. These changes may be responsible for strong fluctuations in the measures of disorder, such as d_d, F_d, m, σ, and $S(1)$. These fluctuations do not behave monotonically; the variation of the amplitude is large for $d_d(\pm21\%)$, $F_d(\pm10\%)$, and $\sigma(8\%)$ and small for $m(0.8\%)$ and $S(1)(\pm1.3\%)$.

In this section, the disorder characteristics in a hexagonal container ($\Gamma=65$) are studied for the stationary states of series-(iii) experiments. Figure 11 shows typical evolutions with ε for the two values of Pr. For all the statistical diagnostics used, the variation with ε is linear for the low-viscosity silicon oil, in the considered range of instability [Figs. 11(a), 11(c), and 11(d)]. Only the variation of d_d is linear at higher viscosity [Fig. 11(a)], topological disorder at high Pr being larger than that at low Pr. It follows from the statistical analysis of array organization by the MST method that the representative points at ε about 10 fall in the (m,σ) plane near the trajectory H-RD joining the perfect hexagonal array to the random distribution [Fig. 11(b)]. Yet, the influence of Pr is noticeable at lower values. For Pr_1, the evolution of the representative point stays along the H-RD line with a continuous enhancement of Gaussian disorder (m decreases and σ increases). For Pr_2, there is, in the beginning, some oscillatory behavior around the H-RD line. The dissimilarity between the two fluids is furthermore stressed by the different aspects of F_d and $S(1)$, which, for Pr_2, both reach an asymptotic value at higher ε [Figs. 11(c) and 11(d)].

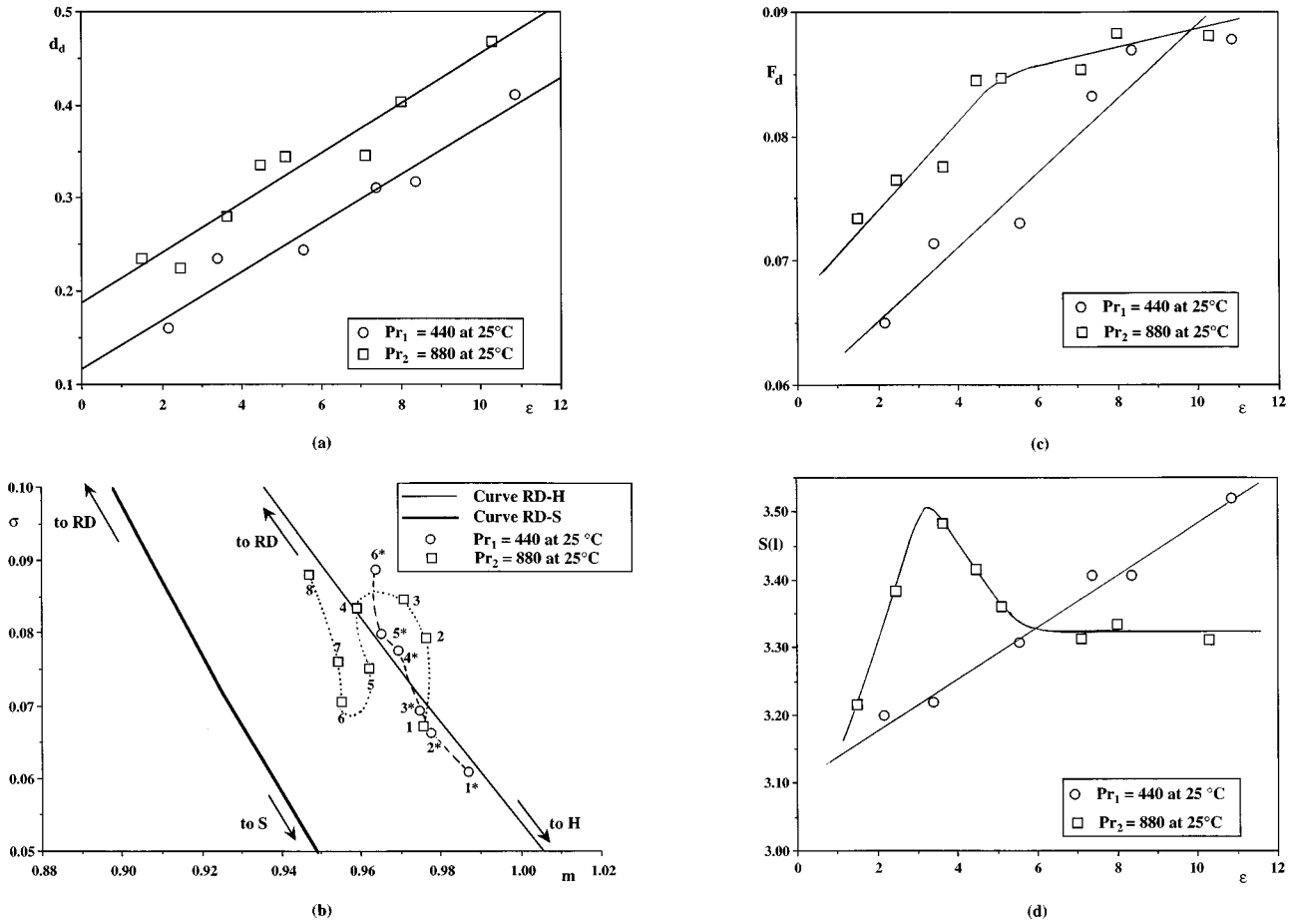

FIG. 11. Variation with the distance from the threshold ε of disorder characteristics of series-(iii) experiments. Peripheral cells are excluded from calculations. (a) Density of defects d_d; (b) evolution in the (m,σ) diagram, the values of ε are 2.1, 3.4, 5.5, 7.4, 8.4, and 10.8 in order of increasing numbers for Pr_1 and 1.5, 2.5, 3.6, 4.5, 5.1, 7.1, 8, and 10.3 for Pr_2; (c) disorder function F_d; and (d) entropy $S(l)$. In (b) the lines serve as guides to the eye.

Whereas F_d continuously goes to saturation, the variation of edge-length entropy $S(1)$ first goes through a maximum concomitant to the oscillation in the (m,σ) diagram.

The origin of the differences between Pr_1 and Pr_2 has probably to be sought in the larger viscous drag that occurs at higher viscosity, which makes more nonlocal the adjustments in the pattern. Such long-range effects are likely to impede global ordering, as an improvement in some place might destroy some farther area already organized. Such a process would be a permanent source of disorder. It would explain why, at low ε, the histograms of angles reveal a marked difference between Pr_1 and Pr_2, the disorientation being already complete in the latter case [Fig. 12(b)]. This observation is also true for the center-to-center distance histograms whose standard deviations at $\varepsilon \approx 1.8$ are 0.052 and 0.146 for Pr_1 and Pr_2, respectively.

V. CONCLUSION

We have carried out a quantitative statistical analysis of the influence of two critical external parameters, namely, vessel geometry and initial conditions, on the array dynamics and amount of disorder of Bénard-Marangoni convective patterns. Experimental results confirm that vessels with a shape that favors hexagonal symmetry (hexagonal, cylindrical) minimize disorder. The imposed regular hexagonal pattern can survive only in a hexagonal vessel and only if the imposed wavelength is equal to the natural one corresponding to the Rayleigh number. In all other cases, the forced planform does not remain stable and, from the various initial states we have imposed, evolves to the same final disordered structure. The superposition ''cellular array=honeycomb +Gaussian noise'' is recovered. The result of the present study, ''limited dynamics=limited disorder,'' which led us to conjecture that ''no dynamics=no disorder,'' suggests

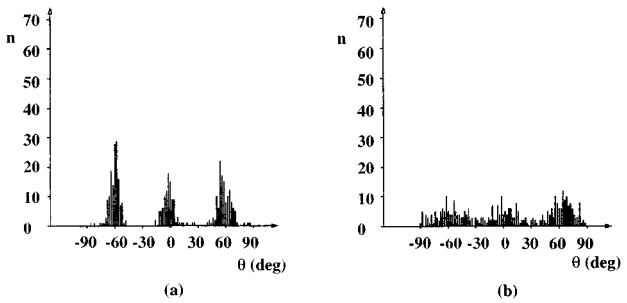

FIG. 12. Histograms of MST angles for series (iii). Peripheral cells are excluded from calculations. (a) Pr_1, $\varepsilon=2.1$; (b) Pr_2, $\varepsilon=1.5$.

that this superposition actually is a generic feature, the physical origin of noise being the dynamics of pattern formation and selection itself. The MST approach thus appears to be a sound method for the study of disorder in 2D convective patterns, providing qualitative and quantitative information on array disorder, in particular to check if order is hidden behind disorder.

Yet, conclusions remain limited by the fact that, except when the experimental point coincides with some reference arrangement or trajectory, a measure of the distances in the (m,σ) plane is up to now lacking. This gap might be filled by introducing an appropriate entropy function. To our knowledge, it is the first time that the edge-length entropy $S(1)$ has been checked in experiments. Results are in conformity with thermodynamics and experience gotten from direct observation, so that $S(l)$ looks very promising for establishing a hierarchy of the BM patterns and others.

The main result from the investigation of the evolution of the patterns with the distance from the threshold and the Pr number of the fluid seems to be the role of viscous drag effects, which, by long-range influence, feed disorder back into the array.

[1] M. C. Cross and P. C. Hohenberg, Rev. Mod. Phys. **65**, 3 (1993).

[2] S. Ciliberto and P. Bigazzi, Phys. Rev. Lett. **60**, 286 (1988); M. Caponeni and S. Ciliberto, Physica D **58**, 365 (1992).

[3] N. B. Tufillaro, R. Ramshankar, and J. P. Gollub, Phys. Rev. Lett. **62**, 422 (1989).

[4] M. Dubois, F. Daviaud, and M. Bonettie, Phys. Rev. A **42**, 3388 (1990).

[5] S. W. Morris, E. Bodenschatz, D. S. Cannel, and G. Ahlers, Phys. Rev. Lett. **71**, 2026 (1993).

[6] P. Bergé and M. Dubois, in *Systems Far from Equilibrium*, edited by L. Garrido (Springler-Verlag, Berlin, 1980).

[7] A. C. Newell and J. A. Whitehead, J. Fluid Mech. **38**, 279 (1969); M. C. Cross, Phys. Rev. A **25**, 1065 (1982).

[8] P. Cerisier, C. Jamond, J. Pantaloni, and C. Perez-Garcia, Phys. Fluids **30**, 954 (1987).

[9] J. Pantaloni and P. Cerisier, in *Cellular Structures in Instabilities*, edited by J. E. Wesfreid and S. Zaleski (Springler-Verlag, Berlin, 1984).

[10] H. Jamgotchian, B. Billia, and L. Capella, J. Cryst. Growth **64**, 338 (1983).

[11] P. Cerisier, R. Occelli, C. Pérez-Garcia, and C. Jamond, J. Phys. (Paris) **48**, 569 (1987).

[12] P. Cerisier and M. Zouine, Phys. Chem. Hydrodynam. **11**, 659 (1989).

[13] P. Cerisier, Phys. Fluids A **3**, 2061 (1991).

[14] J. Toner and D. R. Nelson, Phys. Rev. B **23**, 316 (1981); J. M. Dreyfus and E. Guyon, J. Phys. (Paris) **42**, 283 (1981).

[15] R. Occelli, E. Guazzelli, and J. Pantaloni, J. Phys. (Paris) Lett. **44**, L-567 (1982).

[16] A. Pocheau and V. Croquette, J. Phys. **45**, 489 (1984).

[17] Y. Pomeau and P. Manneville, Phys. Lett. A **75**, 296 (1980).

[18] Y. Pomeau and S. Zaleski, J. Phys. **42**, 515 (1981).

[19] P. Cerisier, H. Nguyen Thi, and B. Billia, Physica D **61**, 113 (1992).

[20] C. Dussert, G. Rasigni, M. Rasigni, J. Palmari, and A. Liebaria, Phys. Rev. B **34**, 3528 (1986).

[21] B. Billia, H. Jamgotchian, and H. Nguyen Thi, Metall. Trans. A **22**, 3041 (1991); Q. Li, H. Nguyen Thi, H. Jamgotchian, and B. Billia, Acta Metall. Mater. **43**, 1271 (1995).

[22] P. Cerisier, C. Perez-Garcia, C. Jamond, and J. Pantaloni, Phys. Rev. A **35**, 1949 (1987).

[23] P. Cerisier, J. Pantaloni, and C. Pérez-Garcia, Phys. Chem. Hydrodynam. **10**, 34 (1988).

[24] *Ordering in Two Dimensions*, edited by S. K. Sinha (North-Holland, Amsterdam, 1980), p. 126.

[25] F. Harary, R. Z. Norman, and D. Cartwight, *Structural Models* (Wiley, New York, 1965).

[26] C. T. Zahn, IEEE Trans. Comput. **20(c)**, 66 (1971).

[27] C. Dussert, Ph.D. thesis, University of Aix-Marseille III, Marseille, France, 1988 (unpublished).

[28] M. Duneau and A. Katz, Phys. Rev. Lett. **54**, 2688 (1985).

[29] A. Loeffler, Diplôme d'Etudes Supérieures, University of Aix-Marseille III, Marseille, France, 1992 (unpublished).

[30] S. Zaleski, Ph.D. thesis, University of Paris, Paris, France, 1980 (unpublished).

[31] Y. Pomeau and P. Manneville, J. Phys. **42**, 1067 (1981).

[32] Y. Pomeau, S. Zaleski, and P. Manneville, Phys. Rev. A **27**, 2710 (1982).

[33] S. H. Davis, J. Fluid Mech. **30**, 465 (1967).

[34] S. H. Davis, J. Fluid Mech. **32**, 619 (1968).

[35] N. Rivier, R. Occelli, J. Pantaloni, and A. Lissowski, J. Phys. **45**, 49 (1984).

[36] M. Kléman, Adv. Phys. **38**, 605 (1989).

[37] J. Sivardière, *La Symétrie en Mathématiques, Physique et Chimie* (Presses Universitaires de Grenoble, Grenoble, France, 1995), Chap. 40.

[38] B. J. Gluckman, P. Marcq, J. Bridger, and J. P. Gollub, Phys. Rev. Lett. **71**, 2034 (1993).

[39] L. Ning, Y. Hu, R. E. Ecke, and G. Ahlers, Phys. Rev. Lett. **71**, 2216 (1993).